Improvements in ECN Wake Model

This paper was presented at the ICOWES2013 Conference, 17-19 June 2013, Denmark

H. Özdemir
M.C. Versteeg (University of Twente)
A.J. Brand

IMPROVEMENTS IN ECN WAKE MODEL

H. Özdemir[1], M.C. Versteeg[2], A.J. Brand[1]

[1]ECN, P.O.Box 1, 1755 ZG Petten, NL, h.ozdemir@ecn.nl
[2]University of Twente, P.O.Box 217, 7500 AE Enschede, NL, m.c.versteeg@student.utwente.nl

INTRODUCTION

Wind turbines extract energy from the flow field so that the flow in the wake of a wind turbine contains less energy and more turbulence than the undisturbed flow, leading to less energy extraction for the downstream turbines. In large wind farms, most turbines are located in the wake of one or more turbines causing the flow characteristics felt by these turbines differ considerably from the free stream flow conditions. The most important wake effect is generally considered to be the lower wind speed behind the turbine(s) since this decreases the energy production and as such the economical performance of a wind farm. The overall loss of a wind farm is very much dependent on the conditions and the lay-out of the farm but it can be in the order of 5-10%. Apart from the loss in energy production an additional wake effect is formed by the increase in turbulence intensity, which leads to higher fatigue loads. In this sense it becomes important to understand the details of wake behavior to improve and/or optimize a wind farm layout. Within this study improvements are presented for the existing ECN wake model which constructs the fundamental basis of ECN's FarmFlow wind farm wake simulation tool [1].

The ECN wake model is called WakeFarm [2, 3, 4] and, based on the original UPMWAKE model proposed by Crespo *et al.* [5, 6], that simulates the wind turbine wakes by solving the steady parabolized Navier-Stokes equations in perturbation form in three-dimensions. The basic background flow is modeled by an atmospheric wind profile model based on Monin-Obukhov similarity theory [7]. The similarity relations suggested by Businger [8] *et al.* are used. Furthermore the perturbation variables are initialized by a near wake model where the parabolization is not justified since the axial-pressure gradient term is neglected.

Schepers [2] pointed out the problem in the near wake and used an empirical velocity-deficit profile as a boundary condition for the far wake. This approach depends on a data-fit with experimental data and the physics of the flow are not modeled explicitly. Schepers and Van der Pijl [4] proposed a model for the near wake based on the free-wake vortex method where the wind turbine is modeled by an actuator disc model and the wake is represented by discrete constant strength vortex rings. They obtained the solution with a panel method. A near wake model is presented here based on a free wake-vortex method as well, where the radius of the

wake and vorticity strength of discrete vortex rings are varied as suggested by Øye [9]. The induced velocities are obtained by a semi-analytical solution of the Biot-Savart law.

The diabatic wind profiles for the surface layer of the atmospheric boundary layer have been investigated extensively [8, 10]. The atmospheric stability model based on Monin-Obukhov [7] theory is only valid within the surface layer of the atmospheric boundary layer. Previous studies [11, 12, 13] show that boundary layer height varies typically between $50 - 200m$ under stable conditions and $500 - 1000m$ under unstable conditions. A need for a model that extends to the entire boundary layer height is obvious considering the sizes of modern wind turbines. Blackadar [14] and Lettau [15] studied a wind shear model covering the entire boundary layer height under neutral condition. Gryning *et al.* [16] extended this model to cover all stability conditions of the atmosphere based on measurements extending in to the mixing layer region where the surface layer scaling is connected with the geostrophic drag law. More recently similar work is done by Peña *et al.* [17]. Sathe *et al.* [18] showed that the loads are predicted smaller with the model proposed by Gryning when compared to models based only on surface layer wind profiles.

Within this study the ECN wake model is extended further based on the model proposed by Gryning *et al.* [16]. The numerical solution obtained by the ECN wake model using Gryning model is compared with the solution obtained by surface layer model and with the available data obtained by EWTW measurements.

The outline of this paper is as follows: First of all the governing equations of the ECN wake farm model are presented. Then the near wake modeling is discussed and the results compared with the original near wake modeling and EWTW data as well as the results obtained for various near wake implementation cases are shown. The details of the atmospheric stability model are given and the comparison with the solution obtained for the original surface layer model and with the available data obtained by EWTW measurements are presented. Finally the conclusions are summarized.

GOVERNING EQUATIONS

In the wake model originally proposed by Crespo *et al.* [5] the wind turbine is supposed to be immersed in a nonuniform basic flow corresponding to the surface layer of the atmospheric boundary layer. This surface layer which is modeled by the standard surface-layer scaling based on the Monin-Obukhov theory, is assumed to be perturbed by the wind turbine. The equations describing the perturbed flow are obtained by introducing the following perturbation variables in to the Navier-Stokes equations together with the conservation of mass and energy equations and two equations for turbulent kinetic energy and the dissipation rate of the turbulent kinetic energy:

$$u = u' + u_0, \quad v = v', \quad w = w', \quad p = p' + p_0, \quad \theta = \theta' + \theta_0, \quad k = k' + k_0, \quad \varepsilon = \varepsilon' + \varepsilon_0, \quad (1)$$

with u, v, and w are three components of the velocity vector, p is the pressure, θ is the potential temperature, k is the turbulent kinetic energy and ε is the turbulent dissipation rate. Furthermore, the subscript "0" refers to the undisturbed flow and the superscript $()'$ refers to a perturbation variable. This undisturbed flow does not vary in $x-$ and $y-$directions, but does vary in z direction.

For the wake flow behind a wind turbine the following assumptions are made: the streamwise pressure gradient is neglected in the far wake behind the wind turbine while the near wake is modeled by the free-vortex wake model as part of basic background flow. The streamwise diffusion is neglected leading to $\frac{\partial \tau_{ij}}{\partial x} = 0$ and $\nu_t \frac{\partial u_j}{\partial x} = 0$. The undisturbed flow in $y-$ and $z-$ directions is assumed to be zero meaning that the information is only traveling downstream. Furthermore the turbulent stresses can be modeled by Boussinesq's eddy viscosity approximation:

$$\tau_{ij} = \rho \nu_t \left[\frac{u_i}{x_j} + \frac{u_j}{x_i} \right] - \frac{2}{3} \rho k \delta_{ij}. \tag{2}$$

Under these assumption the Navier Stokes equations that describe the flow can be written in parabolized form where the elliptic terms are not present anymore. When the Navier-Stokes equations for the undisturbed flow are subtracted from those equations for the disturbed flow, the following relations can be derived. Please note that the superscript $()'$ is dropped for convenience.

Continuity equation:
$$\frac{\partial u}{\partial x} + \frac{\partial v}{\partial y} + \frac{\partial w}{\partial z} = 0. \tag{3}$$

Momentum equations (x, y and z directions):

$$(u_0 + u)\frac{\partial u}{\partial x} + v\frac{\partial u}{\partial y} + w\frac{\partial (u_0 + u)}{\partial z} = (\nu_t + \nu_{t0})\frac{\partial^2 u}{\partial y^2} + \frac{\partial \nu_t}{\partial y}\frac{\partial u}{\partial y}$$
$$+ (\nu_t + \nu_{t0})\frac{\partial^2 u}{\partial z^2} + \left(\frac{\partial \nu_t}{\partial z} + \frac{\partial \nu_{t0}}{\partial z} \right)\frac{\partial u}{\partial z} + \frac{\partial \nu_t}{\partial z}\frac{\partial u_0}{\partial z} + \nu_t \frac{\partial^2 u_0}{\partial z^2}, \tag{4}$$

$$(u_0 + u)\frac{\partial v}{\partial x} + v\frac{\partial v}{\partial y} + w\frac{\partial v}{\partial z} = -\frac{2}{3}\frac{\partial k}{\partial y} - \frac{1}{\rho}\frac{\partial p}{\partial y} + 2(\nu_t + \nu_{t0})\frac{\partial^2 v}{\partial y^2} + 2\frac{\partial \nu_t}{\partial y}\frac{\partial v}{\partial y}$$
$$+ (\nu_t + \nu_{t0})\frac{\partial^2 v}{\partial z^2} + \left(\frac{\partial \nu_t}{\partial z} + \frac{\partial \nu_{t0}}{\partial z} \right)\frac{\partial v}{\partial z} + \left(\frac{\partial \nu_t}{\partial z} + \frac{\partial \nu_{t0}}{\partial z} \right)\frac{\partial w}{\partial y}, \tag{5}$$

$$(u_0 + u)\frac{\partial w}{\partial x} + v\frac{\partial w}{\partial y} + w\frac{\partial w}{\partial z} = -\frac{1}{\rho}\frac{\partial p}{\partial z} + (\nu_t + \nu_{t0})\frac{\partial^2 w}{\partial y^2} + \frac{\partial \nu_t}{\partial y}\frac{\partial w}{\partial y}$$
$$+ 2(\nu_t + \nu_{t0})\frac{\partial^2 w}{\partial z^2} + 2\left(\frac{\partial \nu_t}{\partial z} + \frac{\partial \nu_{t0}}{\partial z} \right)\frac{\partial w}{\partial z} + \frac{\partial \nu_t}{\partial y}\frac{\partial v}{\partial z} - \frac{2}{3}\frac{\partial (k + k_0)}{\partial z} + \beta g \theta, \tag{6}$$

with β is the expansion coefficient.

Energy equation:

$$(u_0 + u)\frac{\partial \theta}{\partial x} + v\frac{\partial \theta}{\partial y} + \frac{\partial (\theta_0 + \theta)}{\partial z} = (\nu_\theta + \nu_{\theta 0})\frac{\partial^2 \theta}{\partial y^2} + w\frac{\partial \nu_\theta}{\partial y}\frac{\partial \theta}{\partial y}$$
$$+ (\nu_\theta + \nu_{\theta 0})\frac{\partial^2 \theta}{\partial z^2} + \left(\frac{\partial \nu_\theta}{\partial z} + \frac{d\nu_{\theta 0}}{dz} \right)\frac{\partial \theta}{\partial z} + \frac{\partial \nu_\theta}{\partial z}\frac{\partial \theta_0}{\partial z} + \nu_\theta \frac{\partial^2 \theta_0}{\partial z^2}. \tag{7}$$

Turbulent kinetic energy:

$$(u_0+u)\frac{\partial k}{\partial x}+v\frac{\partial k}{\partial y}+w\frac{\partial (k_0+k)}{\partial z} = (\nu_k+\nu_{k0})\frac{\partial^2 k}{\partial y^2}+\frac{\partial \nu_k}{\partial y}\frac{\partial k}{\partial y}+(\nu_k+\nu_{k0})\frac{\partial^2 k}{\partial z^2}$$

$$+\left(\frac{\partial \nu_k}{\partial z}+\frac{d\nu_{k0}}{dz}\right)\frac{\partial k}{\partial z}+\frac{\partial \nu_k}{\partial z}\frac{\partial k_0}{\partial z}+\nu_k\frac{\partial^2 k_0}{\partial z^2}+(\nu_t+\nu_{t0})\left[\left(\frac{\partial u}{\partial y}\right)^2+\left(\frac{\partial u}{\partial z}\right)^2+2\frac{\partial u}{\partial z}\frac{\partial u_0}{\partial z}\right]$$

$$+\nu_t\left(\frac{du0}{dz}\right)^2-\beta g\nu_\theta\left(\frac{\partial \theta}{\partial z}+\frac{\partial \theta_0}{\partial z}\right)-\beta g\nu_{\theta 0}\frac{\partial \theta}{\partial z}-\varepsilon. \tag{8}$$

Dissipation rate of the turbulent kinetic energy:

$$(u_0+u)\frac{\partial \varepsilon}{\partial x}+v\frac{\partial \varepsilon}{\partial y}+w\frac{\partial (\varepsilon_0+\varepsilon)}{\partial z} =$$

$$(\nu_\varepsilon+\nu_{\varepsilon 0})\frac{\partial^2 \varepsilon}{\partial y^2}+\frac{\partial \nu_\varepsilon}{\partial y}\frac{\partial \varepsilon}{\partial y}+(\nu_\varepsilon+\nu_{\varepsilon 0})\frac{\partial^2 \varepsilon}{\partial z^2}+\left(\frac{\partial \nu_\varepsilon}{\partial z}+\frac{d\nu_{\varepsilon 0}}{dz}\right)\frac{\partial \varepsilon}{\partial z}+\frac{\partial \nu_\varepsilon}{\partial z}\frac{\partial \varepsilon_0}{\partial z}+\nu_\varepsilon\frac{\partial^2 \varepsilon_0}{\partial z^2}$$

$$+C_{\varepsilon_1}\frac{\varepsilon_0+\varepsilon}{k_0+k}(\nu_t+\nu_{t0})\left[\left(\frac{\partial u}{\partial y}\right)^2+\left(\frac{\partial u}{\partial z}\right)^2+\left(\frac{\partial u_0}{\partial z}\right)^2+2\frac{\partial u}{\partial z}\frac{\partial u_0}{\partial z}-(1-C_{\varepsilon_3})\beta g\frac{1}{\sigma_\theta}\frac{\partial (\theta+\theta_0)}{\partial z}\right]$$

$$-C_{\varepsilon_1}\frac{\varepsilon_0}{k_0}\nu_{t0}\left[\left(\frac{\partial u_0}{\partial z}\right)^2-(1-C_{\varepsilon_3})\beta g\frac{1}{\sigma_\theta}\frac{\partial \theta_0}{\partial z}\right]-C_{\varepsilon_2}\frac{(\varepsilon+\varepsilon_0)^2}{k+k_0}+C_{\varepsilon_2}\frac{\varepsilon_0^2}{k_0}, \tag{9}$$

with,

$$\nu_t=C_\mu\frac{(k+k_0)^2}{\varepsilon+\varepsilon_0}-\nu_{t0}, \quad \nu_\theta=\frac{\nu_t}{\sigma_\theta}, \quad \nu_k=\frac{\nu_t}{\sigma_k}, \quad \nu_\varepsilon=\frac{\nu_t}{\sigma_\varepsilon}. \tag{10}$$

where C_μ, C_{ε_1}, C_{ε_2}, C_{ε_3}, σ_θ, σ_k and σ_ε are the closure coefficients of the system. The system of equations given between equation (3) and (9) form a steady, three-dimensional parabolic set of equations. These equations are discretized with central differences and integrated employing the semi-implicit ADI scheme. The pressure is evaluated using the SIMPLE method [19].

Dirichlet and Neumann boundary conditions are applied at boundaries of the domain [6]. The numerical values are determined from the undisturbed flow in front of the wind turbine.

The solution domain size is chosen to be at least ten times the wind turbine diameter, D, along $x-$ direction (i.e., downstream wake direction) and six times the wind turbine diameter in $y-$ and $z-$directions. A grid stretching is applied along the $x-$direction within the near-wake region. For a typical simulation of a single turbine-single wake combination around $1\cdot 10^6$ grid points are used.

NEAR WAKE MODEL

In the original ECN wake model the near wake is modeled by a free-wake vortex model where the vorticity strength of vortex rings are kept constant while the wake radius is varied. The solution is obtained by a panel method. In the current study the near-wake model is improved further as suggested by Øye [9]. The wind turbine rotor is modeled by an actuator disc model and the wake is represented by a thin vortex sheet which is described by vortex rings of variable

radius and variable vorticity strength leading to a variable transport velocity at infinity. Flow is assumed to be axisymmetric. Induced velocity profiles are obtained analytically using Biot-Savart law, where the elliptic integrals are evaluated numerically. The radii along the wake are calculated by making use of the continuity equation and the solution is iterated until convergence is reached between the local radius and the vorticity.

In figure (1) a comparison of various calculation methods that have been studied and the original panel method are presented. The wake radius is plotted against the distance from the turbine in downstream direction for constant vortex strength (Γ) and variable vortex strength cases for uniform and stretched grid distributions. All results are obtained for an axial induction factor of 0.28. The left-hand side of the figure is a close-up of the near-wake region while on the right-hand side the full domain is presented. In figure (2) the induced velocity just behind the rotor is
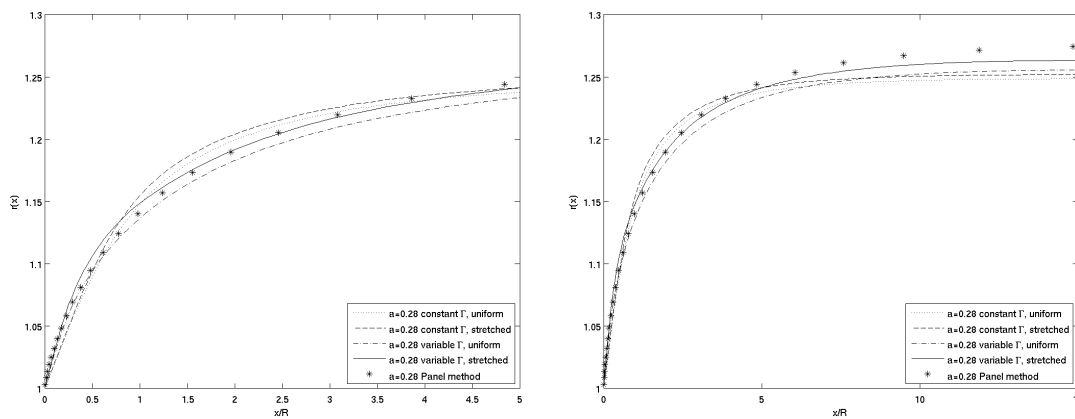

Figure 1: Comparison of the wake radius as a function of distance from the turbine up to $5R$ (left) and $15R$ (right) with $a = 0.28$, as simulated by the constant vorticity vortex ring model, the variable vorticity vortex ring model and the panel method. The new near wake models are simulated on uniform and stretched grids.

shown for the panel method and the variable vorticity vortex ring method for an axial induction factor of 0.28. It is clear that the models are comparable, but that inside the wake the induced velocity in downstream direction is higher in an absolute sense. According to actuator disc momentum theory the induced velocity just behind the rotor is $-aU_\infty$, so the variable vorticity vortex ring model agrees better with the theory. The results of both original and new wake models are compared with the experimental data obtained from the measurements at ECN Wind turbine Test field Wieringermeer, EWTW. The test site consists of five state of the art turbines in a row, a scaled wind farm with 10 wind turbines of 7.5 meter hight and 7.6 meter in diameter and 5 prototype spots for certification of industrial turbines. The five state of the art turbines, with a hub height and diameter of 80 meters, are situated in a row and a meteorological measurement mast is located in the proximity of T5 and T6, as can be seen on the left-hand side of figure (3) [20]. Since there is only one measured point in the field, multiple measurements are combined to get the horizontal wake profile behind a turbine on a certain distance. The right-hand side of
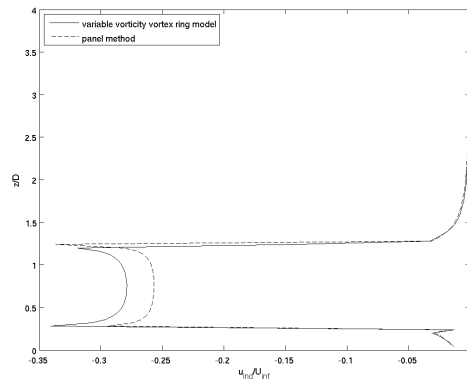
Figure 2: Comparison of velocity and force profiles just behind the rotor plane at the symmetry plane, as simulated by the variable vorticity vortex ring model (the new near wake model) and the panel method (the old near wake model).

figure (3) shows the distance S between the mast and the wind turbines: 2.5D and 3.5D. When the wind direction is 31 degrees or 315 degrees the velocity at the wake center is measured. When the wind comes from a different direction, the distance y to the wake center is calculated. The results of the numerical simulation obtained by the ECN wake model WakeFarm using the
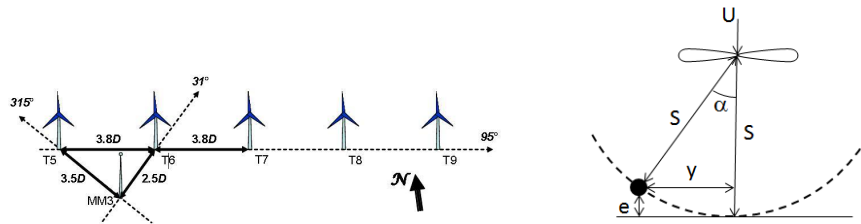

Figure 3: Location of wind turbines and meteorological measurement mast at EWTW (left). When the turbine yaws the meteorological mast moves along the dashed line with respect to the rotor (right).

original (panel method) and new near wake models are compared with the EWTW data and shown in figure (4). WakeFarm performs best at 2.5D, but for 3.5D the results deviate more from the experimental measurements. For the details of the experimental work one is referred to reference [20].

ATMOSPHERIC BOUNDARY LAYER STABILITY MODEL

In the original UPMWAKE model of Crespo *et al.* [5] a diabatic wind profile based on Monin-Obukhov [7] similarity theory and Businger *et al.* [8] formulation is used given as follows:

$$u = \frac{u_{*0}}{\kappa} \left[\ln \left(\frac{z}{z_0} \right) - \psi_m \left(z/L \right) \right], \tag{11}$$
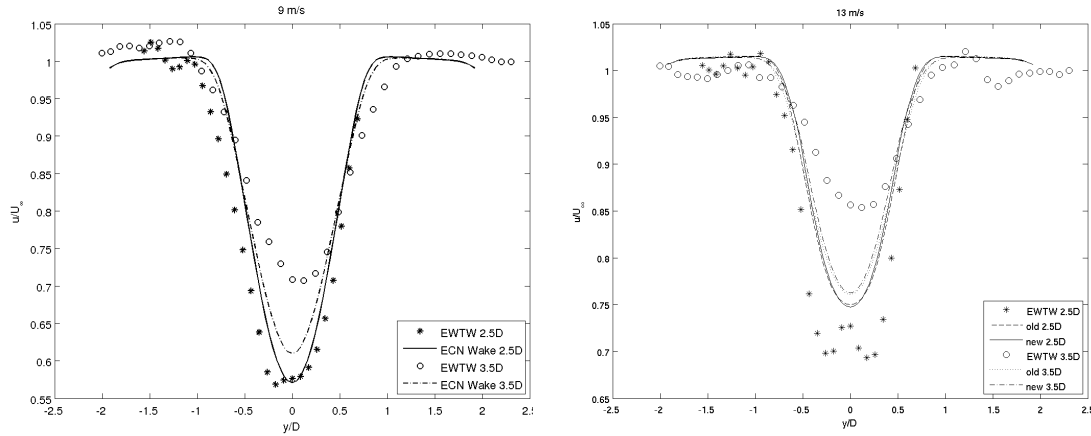
Figure 4: Comparison of EWTW experimental data with velocity profiles in wake direction, as simulated by ECN wake model using the original and the new near wake model, respectively.

where u_{*0} is the friction velocity near the ground, z is the height, z_0 is the aerodynamic roughness length, κ is the von Kármán constant, L is the Monin-Obukhov length and ψ_m is a universal stability function which is defined empirically. In the original ECN wake model the above wind profile is adopted whith the Bussinger *et al.* [8] form for stability function ψ_m where further details are given by Panofsky and Dutton [21]. The Monin-Obukhov length, L, is given by the following expression:

$$L = \frac{u_{*0}^3 T}{\kappa g \overline{\omega' \theta_0'}},$$

(12)

where, T is the absolute temperature, θ_0 is the potential temperature and $\overline{\omega' \theta_0'}$ is the virtual kinematic heat flux.

The diabatic wind profile models using surface layer scaling of Monin-Obukhov [7] are valid only within the surface layer of the atmosphere. In the current study the extended wind profile model proposed by Gryning *et al.* [16] is used which is valid for the entire boundary layer. The model is given as follows:

For neutral conditions:

$$u = \frac{u_{*0}}{\kappa} \left[\ln \left(\frac{z}{z_0} \right) + \frac{z}{L_{MBL}} - \frac{z}{z_i} \left(\frac{z}{2L_{MBL}} \right) \right],$$

(13)

for unstable conditions:

$$u = \frac{u_{*0}}{\kappa} \left[\ln \left(\frac{z}{z_0} \right) - \psi_m \left(z/L \right) + \frac{z}{L_{MBL}} - \frac{z}{z_i} \left(\frac{z}{2L_{MBL}} \right) \right],$$

(14)

	Unstable	Neutral	Stable
L	-128 m	321 m	41 m
z_i	117 m	205 m	49 m
L_{MBL}	283 m	866 m	69 m

Table 1: Parameters used for figure (5)

for stable conditions:

$$u = \frac{u_{*0}}{\kappa}\left[\ln\left(\frac{z}{z_0}\right) - \psi_m\left(z/L\right)\left(1 - \frac{z}{2z_i}\right) + \frac{z}{L_{MBL}} - \frac{z}{z_i}\left(\frac{z}{2L_{MBL}}\right)\right], \tag{15}$$

with z_i is the height of the atmospheric boundary layer and defined as follows for the neutral conditions [22]:

$$z_i = c\frac{u_{*0}}{|f|} \tag{16}$$

with c is a constant and f is the Coriolis parameter. The value of c is adopted from the works of Sathe *et al.* [18] and Peña *et al.* [23, 24] as 0.15 for neutral conditions, 0.14 for stable conditions and 0.13 for very stable conditions.

Stability function, ψ_m, is used from Businger *et al.* [8] for stable conditions and from Grachev *et al.* [10] for unstable conditions. An empirical fit suggested by Gryning *et al.* [16] for the scaling parameter, L_{MBL}, is in the following form:

$$\frac{u_{*0}}{fL_{MBL}} = \left(-2\ln\left(\frac{u_{*0}}{fz_0}\right) + 55\right)e^{\left(-\frac{(u_{*0}/fL)^2}{400}\right)}. \tag{17}$$

In figure (5) the influence of various models for an atmospheric boundary layer velocity profile is presented using the parameters listed in table (1). It can also be concluded from these figures that the choice for the atmospheric boundary layer stability model is most important for (very) stable conditions.
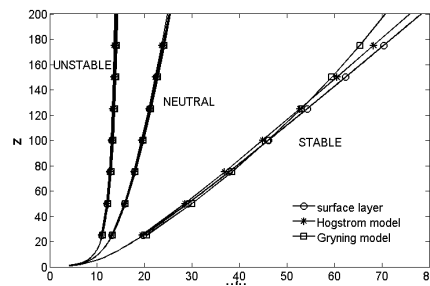

Figure 5: Influence of the atmospheric boundary-layer model on the velocity profile for unstable, neutral and stable conditions.
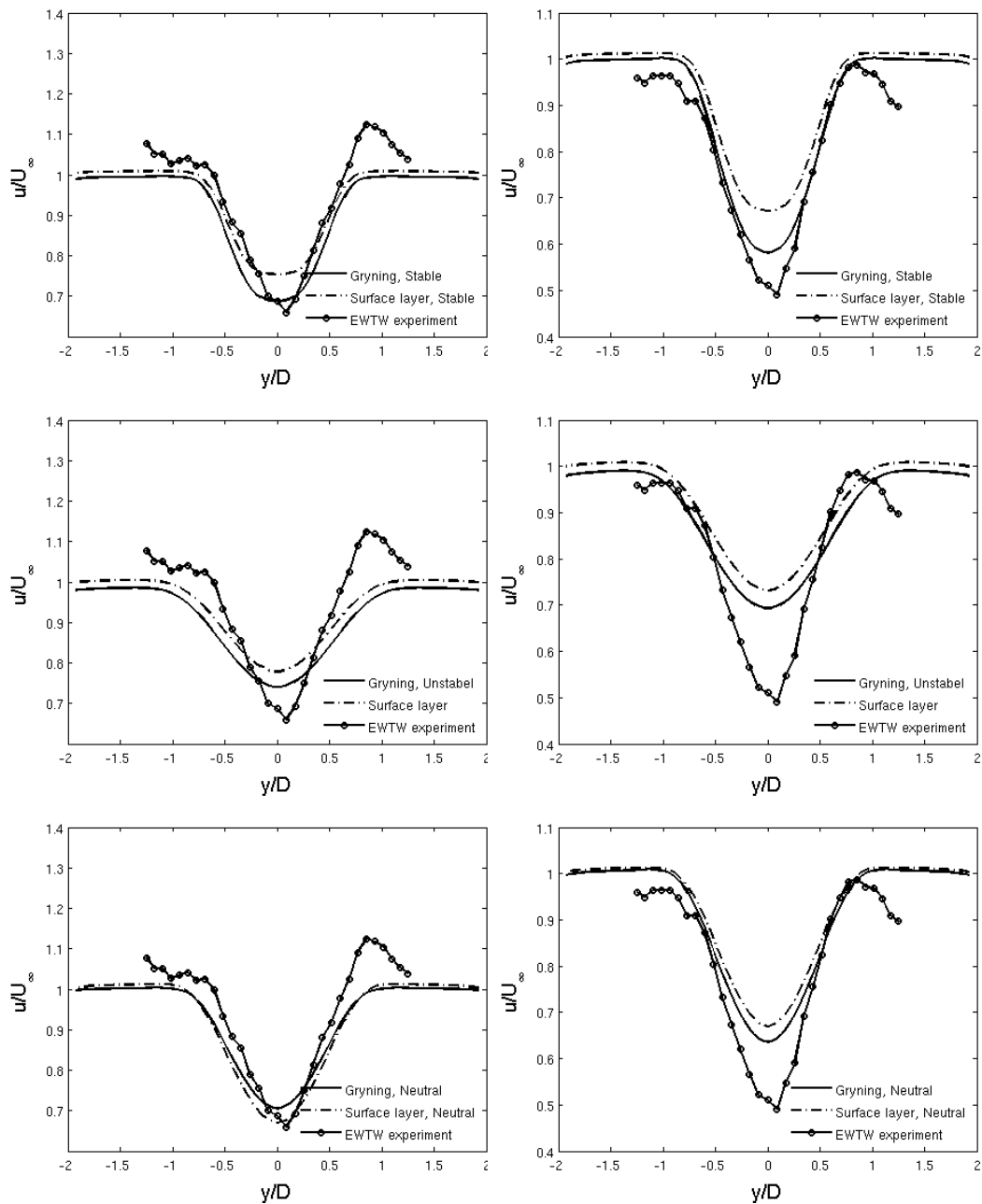
Figure 6: Comparison of numerical simulation using Gryning *et al.* [16] model for stable, neutral and unstable conditions with the surface layer model and the available data from EWTW measurements for $U_\infty = 8m/s$ (left) and $U_\infty = 10m/s$ (right).

Sathe *et al.* [18] showed the importance of using a diabatic wind profile for the entire boundary layer. They argued that using a surface layer model predicts the blade and rotor loads along the

wake direction much larger compared to a model for the entire boundary layer particularly for stable conditions, since in the surface-layer wind profile model under stable conditions, the wind profile length scale increases infinitely, leading to large wind gradients, while a wind profile for the entire boundary layer [16] limits the growth of this length scale using the boundary layer height, leading to smaller wind shear.

In figure (6) a comparison of numerical simulation using Gryning *et al.* [16] model valid for the entire boundary layer for stable, neutral and unstable conditions with the surface layer model and the available data from EWTW measurements for $U_\infty = 8m/s$ (left) and $U_\infty = 10m/s$ (right) is given. The EWTW data is evaluated as described in the previous section. The induced velocity is predicted lower compared to the surface layer model which is in agreement with Sathe *et al.* [18]. It should be noted here that a single EWTW data set is used for the entire stability region and the simulation results for each stability region are compared with this single data.
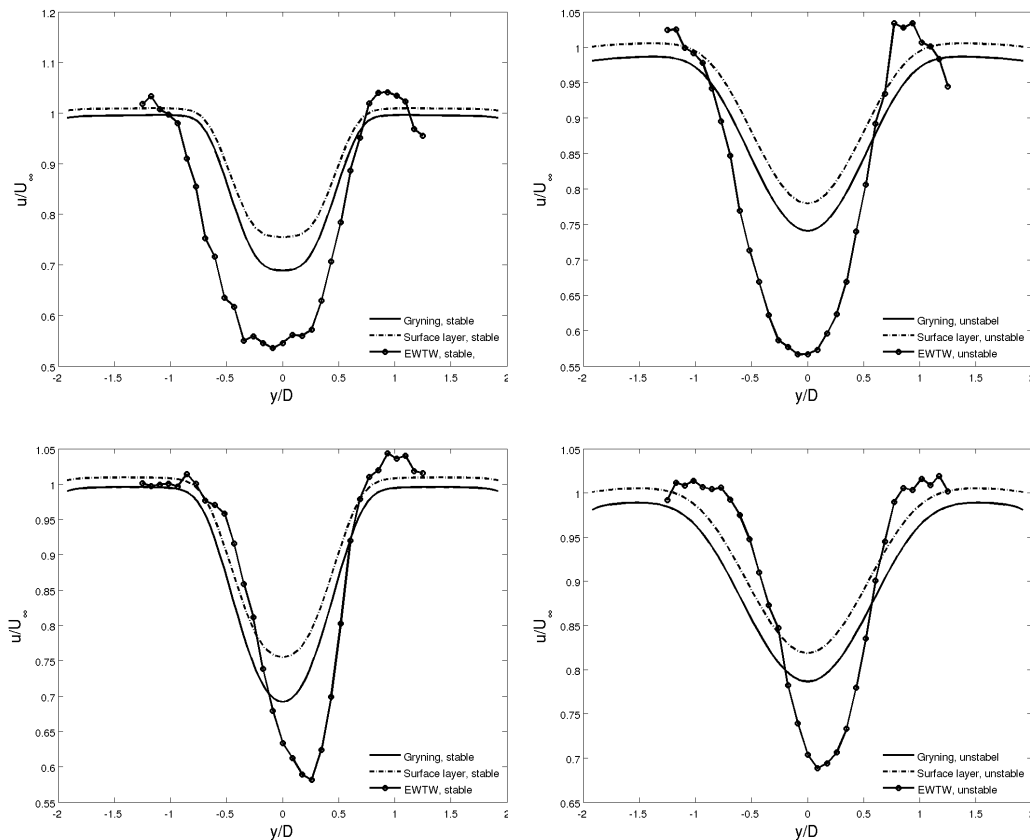

Figure 7: Comparison of numerical simulation using Gryning *et al.* [16] model with the surface layer model and the data from EWTW measurements for stable and unstable conditions for $U_\infty = 8m/s$, at $2.5D$ (left) and $3.5D$ (right).

There is a necessity of determination of the experimental data for various stability conditions.

The available EWTW data do not contain any information to categorize the stability of the atmosphere at the moment of the measurements. In the literature there are several rough estimates are given about the estimation of the stability condition of the atmosphere depending on the time of the day [22]. Based on these rough estimates the data measured between sunrise and sunset is assumed to be unstable and between sunset and sunrise is assumed to be stable. The comparison of the numerical simulation using Gryning *et al.* [16] model with the surface layer model and the data from EWTW measurements for stable and unstable conditions for $U_\infty = 8m/s$ is shown in figure (7) at $2.5D$ and $3.5D$ downstream of the turbine. Although the comparison is not conclusive because of the reliability of the data it is shown here for the demonstration purposes.

CONCLUSIONS

In this study improvements to ECN wake model, WakeFarm, are presented in two folds. First of all, an improved near wake model is shown where the wake is modeled by a thin vortex sheet represented by discrete vortex rings of variable strength. The solution is obtained analytically with the Biot-Savart law, where the elliptic integrals are evaluated numerically. It is shown that the induced velocity is lower than for the original near wake model, which is in accordance with the theory. Furthermore the diabatic wind profile model is improved by implementing a model valid for the entire boundary layer as suggested by Gryning *et al.* [16]. The results are compared with a diabatic wind model valid for the surface layer and with the data obtained from EWTW measurements. Although the results seem closer to the data, the EWTW data is a single data set representing all stability regions. An initial attempt to categorize the EWTW data in to two stability regions depending on the time of the day of the measured data did not lead to better conclusions. A need for a better data mining to distinguish the different stability regions and data from different sites is obvious. In addition, accurate temperature measurements should be standard for wake measurement campaigns.

ACKNOWLEDGMENTS

REFERENCES

[1] FarmFlow, "http://www.ecn.nl/nl/units/wind/rd-programma/aerodynamica/windfarm-aerodynamics/farmflow/," 2013.

[2] J. G. Schepers, "Wakefarm: nabij zog model en ongestoord wind snelheidsveld," Tech. Rep. ECN-C–98-016, ECN, 1998.

[3] S. P. van der Pijl and J. G. Schepers, "Improvements of the wakefarm wake model," in *Workshop on wake modelling and benchmarking of models, Annex XXIII: Offshore wind energy technology and deployment*, (Billund), 2006.

[4] J. G. Schepers and S. P. van der Pijl, "Improved modelling of wake aerodynamics and assessment of new farm control strategies," in *The Science of Making Torque from Wind*, Journal of Physics: Conference series 75, 2007.

[5] A. Crespo, F. Manuel, D. Moreno, F. Fraga, and J. Hernáandez, "Numerical analysis of wind turbine wakes," in *Delphi Workshop on Wind turbine applications*, 1985.

[6] A. Crespo and J. Hernández, "Numerical modelling of the flow field in a wind turbine wake," in *3rd Joint ASCE/ASME Mechanics Conference*, 1989.

[7] A. S. Monin and A. M. Obukhov, "Basic laws of turbulent mixing in the surface layer of the atmosphere," *Tr. Akad. Nauk SSSR Geofiz. Inst.*, vol. 24, pp. 163–187, 1954. English translation by John Miller, 1959.

[8] J. A. Businger, J. C. Wjngaard, Y. Izumi, and E. F. Bradley, "Flux-profile relationships in the atmospheric surface layer," *Journal of the Atmospheric Sciences*, vol. 28, pp. 181–189, 1971.

[9] S. Øye, "A simple vortex model," in *3rd IEA Symposium on the Aerodynamics of Wind Turbines*, pp. 4.1–4.15.

[10] A. Grachev, C. Fairall, and E. Bradley, "Convective profile constants revisited," *Boundary-Layer Meteorology*, vol. 94, no. 3, pp. 495–515, 2000.

[11] P. Seibert, F. Beyrich, S. Gryning, S. Joffre, A. Rasmussen, and P. Tercier, "Review and intercomparison of operational methods for the determination of the mixing height," *Atmospheric Environment*, vol. 34, no. 7, pp. 1001 – 1027, 2000.

[12] M. A. Gárcia, M. L. Sánchez, B. de Torre, and I. A. Pérez, "Characterisation of the mixing height temporal evolution by means of a laser dial system in an urban area intercomparison results with a model application," *Ann. Geophys.*, vol. 25, p. 21192124, 2007.

[13] S. Emeisa, C. Münkelb, S. Vogtc, W. Müllerd, and K. Schäfera, "Atmospheric boundary-layer structure from simultaneous sodar, rass, and ceilometer measurements," *Atmospheric Environment*, vol. 38, no. 2, pp. 273–286, 2004.

[14] A. Blackadar, "The vertical distribution of wind and turbulent exchange in a neutral atmosphere," *Journal of Geophysical Research*, vol. 67, no. 8, pp. 3095–3102, 1962.

[15] H. Lettau, "Studies of the three-dimensional structure of the planetary boundary layer," Tech. Rep. AD-296160, University of Wisconsin, Department of Meteorology, 1962.

[16] S. E. Gryning, E. Batchvarova, B. Brümmer, H. Jørgensen, and S. Larsen, "On the extension of the wind profile over homogeneous terrain beyond the surface boundary layer," *Boundary-Layer Meteorology*, vol. 124, no. 2, pp. 251–268, 2007.

[17] A. Peña, S. E. Gryning, and C. B. Hasager, "Comparing mixing-length models of the diabatic wind profile over homogeneous terrain," *Theoretical and Applied Climatology*, 2010.

[18] A. Sathe, J. Mann, T. Barlas, W. A. A. M. Bierbooms, and G. J. W. van Bussel, "Influence of atmospheric stability on wind turbine loads," *Wind Energy Journal*, vol. DOI:10.1002/we.1528, 2012.

[19] S. V. Patankar and D. B. Spalding, "A calculation procedure for heat, mass and momentum transfer in three-dimensional parabolic flows," *Int. J. Heat Mass Transfer*, 1972.

[20] L. A. H. Machielse, P. J. Eecen, S. P. van der Pijl, and J. G. Schepers, "Ecn test farm measurements for validation of wake models," EWEC, 2007.

[21] H. Panofsky and J. Dutton, *Atmospheric Turbulence*. John Wiley and Sons, 1984.

[22] J. R. Garratt, *The atmospheric boundary layer*. Cambridge, 1992.

[23] A. Peña, S. E. Gryning, and C. B. Hasager, "Measurement and modelling of the wind speed profile in the marine atmospheric boundary layer," *Boundary-Layer Meteorology*, vol. 129, pp. 479–495, 2008.

[24] A. Peña, S. E. Gryning, J. Mann, and C. B. Hasager, "Length scales of the neutral wind profile over homogeneous terrain," *Journal of Applied Meteorology and Climatology*, vol. 49, pp. 792–806, 2010.